Modeling and Simulation of a Laser-Powered Lightcraft Using Impulse State-Time Equations

John A. Evans,* Mojtaba Oghbaei,*and Kurt S. Anderson†
Rensselaer Polytechnic Institute, Troy, New York 12180, USA

In this paper, the authors demonstrate the capabilities of a novel state-time methodology for the simulation of dynamic systems. The test case under consideration is a six-degree of freedom model of the Type 200 laser-powered lightcraft. The lightcraft problem is a well-suited application demonstrating the potential advantages of using the state-time formulation for achieving significant effective parallel computing utilization as the craft's temporal domain is much larger than its spatial domain. Indeed, while relatively few processors can be effectively utilized in modeling the vehicle via traditional state-type algorithms, more than 10^5 processors may be potentially exploited in a state-time dynamic simulation. In this paper, a modified state-time methodology is derived in order to account for impulsive characteristics. This impulsive formulation allows for parallelization not only between impulses but also across impulses. In fact, this impulsive formulation may be extended towards other dynamic systems exhibiting impulsive behavior as well. Furthermore, an aerodynamic model fully compatibile with the state-time formulation is presented, and a sliding linearization scheme is presented to simplify these resulting terms. A continuation method is utilized along with a Newton-Raphson scheme to solve the resulting system of nonlinear algebraic equations. Validation and verification of the method is obtained by comparing the impulsive state-time simulation results with the results of a traditional state-type dynamics algorithm using Autolev software and with experimental results.

Nomenclature

B : Lightcraft body B
B^* : Center of mass of body B
$\vec{H}^{B/B^*}$: Angular impulse with respect to B^*
$\vec{G}^{B/B^*}$: Linear impulse with respect to B^*
N : Newtonian reference frame
$\vec{I}^{B/B^*}$: Inertia dyadic of the lightcraft with respect to B^*
${}^N\vec{\omega}^B$: Relative angular velocity of the lightcraft
$\dot{\phi}$: Spin rate of the lightcraft relative to the despun reference frame
${}^N\vec{\Omega}^B$: Absolute angular velocity of the lightcraft
${}^N\vec{\alpha}^B$: Absolute angular acceleration of the lightcraft
ε_{ijk} : The standard indicial cyclic permutation operator
$\vec{x}_B$: Displacement vector of B^* with respect to Newtonian reference frame
${}^N\underline{\omega}^B_\times$: Angular velocity cross product matrix
$\underline{C} = {}^N\underline{C}^B$: Direction cosine matrix from the local frame B to N
$\psi_i(t)$: i^{th} members of family of C_0 continuous shape functions
$\bar{x}_{i_\alpha}$: State-time displacement variable
$\bar{q}_{j_\beta}$: State-time angular displacement variable
$\bar{C}_{kl_\gamma}$: State-time direction cosine variable
L, D, M : Aerodynamic lift, drag, and pitching moment with respect to B^*

*Computational Dynamics Laboratory, Department of Mechanical Engineering
†Associate Professor, Computational Dynamics Laboratory, Department of Mechanical Engineering

c_L, c_D, c_M : Coefficients of lift, drag, and pitching moment
ρ : Density of air
S : Planform area
α : Angle of attack

I. Introduction

Computation is quickly establishing itself as a key element in the engineering design process. It saves time, money, and material costs associated with the design, testing, and analysis of prototypes for experimentation. It provides engineers with the necessary tools to effectively utilize theoretical knowledge constituting the governing laws of physical systems. Thus, much effort is spent towards developing faster and more efficient simulation techniques and computational methods. However, one must be careful not to sacrifice accuracy for speed. It is of utmost importance then to test new computational methods for accuracy as well as speed and efficiency.

The presented state-time formulation, which is being developed by the authors,[1,2] is an efficient and highly parallelizable dynamic simulation tool for the analysis of dynamic behavior of multibody systems (MBS). Such systems are collections of interconnected rigid and flexible bodies that can move relative to one another connected by kinematic joints. Systems that can be considered as MBS are quite vast, including air and spacecraft, robot manipulators, nanostructures, microelectromechanical devices, and bio-mechanical systems. A search in literature indicates that MBS become increasingly more complicated due to recent advancements in science and engineering. Thus, there has been a focus in the dynamics community to develop improved methods for modeling and simulation of such systems. The authors' new formulation belongs to this category. The proposed methodology provides the means for exploiting anticipated massively parallel computing resources which could potentially result in significantly reduced dynamic simulation turnaround.

The major problem with many of todays dynamic algorithms is that they are inherently sequential in time. That is, the equations of motion are only parallel within a given temporal integration step. Consequently, as the equations of motion are temporally integrated, all calculations must be done for a given time step before the simulation can move on to the next step. Therefore, increasing the number of available processors in a parallel computing system does not necessarily achieve speedup. Indeed, if not done appropriately, the use of excessive number of processors (beyond some point) will actually slow the simulation down due to high interprocessor communication costs. Thus, prior gains in MBS analysis through the use of parallel computing resources at each time step have been very limited. As the number of temporal steps increase, there is a considerable computational cost in the time domain, which heretofore has not been parallelizable in a general MBS context. In the state-time formulation, time is treated as a variable similar to the system state variables from the finite element point of view. In this sense, the new methodology may be classified as a finite element in time technique. However, the state-time method should not be confused with traditional space-time type finite element methods. In these schemes, the solution variables are interpolated over a small piece of the temporal domain, and the equations of motion are then integrated in a traditional time-marching sense from temporal element to temporal element. In the state-time formulation, on the other hand, time is discretized over the entire length of simulation. As a result of this discretization over the entire temporal and spatial domain, the proposed formulation would allow the equations of motion to be parallelized both temporally and spatially. As such, coarse grain parallelization is made possible within this formulation by distributing a greater number of core calculations over all the available processors, significantly reducing computing time. As parallel computing machines are gaining the ability to harbor ever more processors, this methodology shows great promise for fast and efficient simulation of MBS.

The lightcraft problem is particularly interesting since the course of simulation of this system involves a temporal domain that is much larger than the relatively small 6-DOF spatial domain. Over 10^5 temporal elements or time steps are necessary to properly model the vehicle due to high spin and precession rates. Because of the lightcraft's small spatial domain, relatively few (~ 2) processors can be effectively utilized in modeling the craft with a traditional (state-type) parallel dynamics algorithm. On the other hand, the state-time methodology theoretically allows exploitation of a massive number of processors. This is a significant improvement. The lightcraft problem also introduces some new challenges. As the vehicle is propelled by successive laser impulses, the dynamic formulation would have to account for impulsive characteristics. Thus, in order to model the lightcraft with the state-time methodology, the formulation must be modified

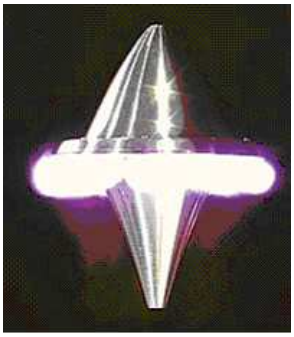

Figure 1. The Type 200 Lightcraft in Flight

accordingly to accommodate for such impulsive loadings and associated velocity jumps. Also, aerodynamics play a key role in the dynamics of the craft. Aerodynamic forces, however, introduce highly nonlinear terms in the resulting equations of motion. An efficient numerical scheme should be developed to deal with this inherent nonlinearity.

II. Lightcraft Basics

The laser-powered lightcraft is an ultra lightweight vehicle powered by repetitively-pulsed detonations induced by a ground-based laser. The Type 200 variant[3] is assembled from three parts: nose, shroud, and rear optic. The parabolically-shaped rear optic is necessary for focusing laser energy into the annular shroud, explosively heating the air and producing thrust. The vehicles consist of very thin shells, about 0.01-inch in thickness, made of 6061-T4 aluminum. The lightcraft is also a body of revolution, being completely symmetric about its spin axis.

The lightcraft receives a propulsive reaction from the laser-induced air detonation within its shroud resulting from a laser pulse. This reaction consists of three linear impulses and three angular impulses, but the impulses applied from a thrust force, side force, and pitching moment dominate the reaction. The thrust impulse propels the vehicle skyward, the side impulse attempts to center the lightcraft in the laser beam, and the pitching impulse, which results from a lateral offset, tends to tip the vehicle. In order to reduce the effects from the pitching impulse, the lightcraft is spun to a speed of approximately 10,000 RPM before it is launched. Though the laser beam hits the lightcraft at a lateral offset, this fact is ignored in the dynamic model discussed in this paper.

An ablative propellent is used to increase the amount of thrust in the laser-supported detonation. This propllent, Delrin, is placed in the inside of the shroud nearest to where the highest temperatures are achieved. This helps to keep the lightcraft shroud from overheating and provides significant additional thrust. At each laser pulse, some of the Delrin ablates, protecting the rear optic from burning through and providing significant additional thrust because of both enhanced gas expansion and mass ejection. The most successful runs of the lightcraft have occurred when Delrin has been successfully utilized.

The lightcraft is currently under development by NASA and is being tested in conjuction with the United States Army and Prof. Leik Myrabo of Rensselaer Polytechnic Institute. Today, it serves as a research craft for designing future light-powered spacecraft. As the laser is ground-based, emphasis may be placed on efficient and economical production of a high quality beam without consideration of weight. Additionally, because the lightcraft does not to a significant degree have to carry its "engine" or fuel, it is theoretically capable of obtaining speeds far greater and more cheaply than through use of chemical propellents.[3] As model based predictive control is eventually required for improved beam-riding performance of the vehicle, development of a fast and efficient dynamic simulation tool for the system is of crucial importance.

III. Overview of the State-Time Formulation

Formulating a problem using the state-time methodology[1,2] involves first writing the variational form of the governing dynamic equations and then applying the Galerkin method of weighted residuals (i.e. the

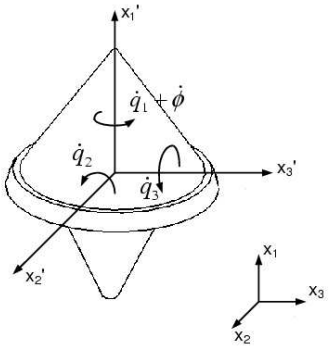

Figure 2. Axis and Variable Definition for the 6-DOF lightcraft Model

interpolation functions are used themselves as the weighting functions). By discretizing the temporal domain in this manner, one is able to treat the time-varying quantities in the equations of motion in a manner identical to the treatment of spatially varying quantities as being done in finite element community. Furthermore, temporal discretization allows one to transform the equations of motion from a set of ordinary/partial differential-algebraic equations to a set of nonlinear algebraic equations which apply over the entire length of simulation. This allows one to completely bypass the serial bottlenecks associated with time-stepping techniques.

In order to produce a system of equations with the least coupling and lowest degree of nonlinearity, a Newton-Euler approach is utilized along with the Poisson's kinematical equations to determine the governing equations of motion. The state-time representation of the above equations results in a large nonlinear algebraic system with only quadratic nonlinearity and light nearest neighbor coupling in the temporal domain. When solving these nonlinear equations with a Newton type approach, one finds the associated tangent matrix is very sparse, banded, and diagonally-dominant. This structure enables parallel iterative sparse solvers to be efficiently and effectively used.

IV. Modified State-Time Formulation

Due to the unique nature of the problem at hand, the state-time equations of motion must be modified to account for special properties of the lightcraft. It should be noted that since this is a free-flying single body problem, no geometric constraint equations need to be included in the state-time formulation.

Additionally, because the lightcraft is spinning at 10,000 RPM, it is unreasonable and computationally expensive to utilize the general form of the Eulers equations. Such a formulation would track a reference frame fixed in the spinning lightcraft body, hence leading to aliasing issues if the temporal mesh utilized was too coarse. Instead, it is convenient to allow the body to rotate about its axis of symmetry relative to a "despun" reference system, as shown in Fig. 2. The Euler's equations are then modified to account for the lightcraft's spin about its axis of symmetry. These modified equations are commonly used in describing tehe dynamic behavior of spinning symmetric bodies and are presented in.[4]

Finally, it is worth mentioning that in traditional state-type dynamic formulations, the equations of motion are integrated until an impulse occurs. Then, the simulation is stopped, and new velocity and angular velocity conditions are determined based on the given impulse conditions. Following the impulse, the simulation resumes and the equations of motion are once again integrated until the next laser pulse occurs. This approach is convenient for traditional dynamic formulations as they are serial in time. For such traditional time marching schemes the system equations of motion must be solved for the state derivatives at the current time step before moving on to the next.

The entire premise for the state-time dynamic formulation, however, is that the equations of motion become parallel in both space and time. Using the modified form of the state-time equations, these equations can still be solved for the entire simulation time in one shot, and no time-stepping maneuvers are necessary. For a low number of impulses, it may be beneficial to solve for the dynamic behavior between impulses

utilizing a state-time formulation, but as the pulse frequency increases (i.e. the time between successive pulses decreases), the advantages of using such a formulation are lost.

Through a clever addition of an "impulse term" to the conventional Newton-Euler equations, one can derive impulse state-time equations of motion which apply throughout the entire time of simulation. This impulse term is created utilizing the Dirac delta function. Through the use of the weak form of the equations of motion, the Dirac delta function is integrated, leaving only a shape function in its final form. The resulting equation is relatively simple to numerically integrate. To demonstrate this process, an impulse state-time treatment of Newton's 2nd Law is presented below.

A. An Impulse State-Time Treatment of Newton's 2nd Law

Consider the Euler's generalization of Newton's 2nd law of motion as given below

$$\sum \vec{F} = m\ddot{\vec{x}} \tag{1}$$

Suppose an impulsive load $\vec{G}$ occurs at $t = t_k$, which can be represented as $\vec{G}\delta(\tau - t_k)$. Then Eqn. (1) can be re-written as

$$\sum \vec{F} + \vec{G}\delta(\tau - t_k) = m\ddot{\vec{x}} \tag{2}$$

Solving for $\ddot{\vec{x}}$ and writing the above equation in weak form over a time interval (t_i, t_f) yields into the following equation

$$\begin{array}{l} \int_{t_i}^{t_{k^-}} \ddot{\vec{x}}\tilde{E}d\tau + \int_{t_{k^-}}^{t_{k^+}} \ddot{\vec{x}}\tilde{E}d\tau + \int_{t_{k^+}}^{t_f} \ddot{\vec{x}}\tilde{E}d\tau = \\ \frac{1}{m}\left\{\int_{t_i}^{tk^-} \vec{F}\tilde{E}d\tau + \int_{t_{k^-}}^{t_{k^+}} \vec{G}\delta(\tau - t_k)\tilde{E}d\tau + \int_{t_{k^+}}^{t_f} \vec{F}\tilde{E}d\tau\right\} \end{array} \tag{3}$$

where $\tilde{E}$ are the weighting or trial functions. Using the approximations

$$\begin{array}{ccc} x_i \to \bar{x}_{i_\alpha}\psi_\alpha(t) & \overset{\text{vel. level}}{\longrightarrow} & \dot{x}_i \to \bar{x}_{i_\alpha}\dot{\psi}_\alpha(t) \\ \tilde{E} \to E_\beta\psi_\beta(t) & \overset{\text{vel. level}}{\longrightarrow} & \dot{\tilde{E}} \to E_\beta\dot{\psi}_\beta(t) \end{array} \tag{4}$$

Eqn. (3) becomes

$$\begin{array}{l} \dot{x}_i\psi_\beta|_{t_i}^{t_{k^-}} - \int_{t_i}^{t_{k^-}} \bar{x}_{i_\alpha}\dot{\psi}_\alpha\dot{\psi}_\beta d\tau + \dot{x}_i\psi_\beta|_{t_{k^-}}^{t_{k^+}} - \int_{t_{k^-}}^{t_{k^+}} \bar{x}_{i_\alpha}\dot{\psi}_\alpha\dot{\psi}_\beta d\tau + \\ \dot{x}_i\psi_\beta|_{t_{k^+}}^{t_f} - \int_{t_{k^+}}^{t_f} \bar{x}_{i_\alpha}\dot{\psi}_\alpha\dot{\psi}_\beta d\tau = \\ \frac{1}{m}\left\{\int_{t_i}^{t_{k^-}} F_i\psi_\beta d\tau + \int_{t_{k^-}}^{t_{k^+}} G_i\delta(\tau - t_k)\psi_\beta d\tau + \int_{t_{k^+}}^{t_f} F_i\psi_\beta d\tau\right\} \end{array} \tag{5}$$

where $\psi_j(t)$ is the j^{th} temporal interpolation function and $\bar{x}_{i_\alpha}$ is the unknown coefficient to be determined. By cancelling terms, noting that G_i is a constant, and noting $\int_{t_{k^-}}^{t_{k^+}} \delta(\tau - t_k)\psi_\beta d\tau = \psi_\beta(t_k)$, Eqn. (5) becomes

$$\dot{x}_i\psi_\beta|_{t_i}^{t_f} - \int_{t_i}^{t_f} \bar{x}_{i_\alpha}\dot{\psi}_\alpha\dot{\psi}_\beta d\tau = \frac{1}{m}\left\{\int_{t_i}^{t_f} F_i\psi_\beta d\tau + G_i\psi_\beta(t_k)\right\} \tag{6}$$

Equation (6) represents the state-time impulse form of the Newton's 2nd Law involving the state-time variable $\bar{x}_{i_\alpha}$ to be determined. Using a similar derivation one can obtain the state-time impulse form of Euler's equations.

B. Lightcraft Equations of Motion

With the preceding considerations, the lightcraft equations of motion are, in vector form,

Euler's Equations

$$\vec{H}_h^{\,B/B^*}\delta(\tau - t_{k_h}) = \vec{I}^{\,B/B^*} \cdot {}^N\vec{\alpha}^B + {}^N\underline{\Omega}^B \times \vec{I}^{\,B/B^*} \cdot {}^N\vec{\omega}^B \tag{7}$$

Newton's 2nd Law

$${}^N\underline{C}^B \cdot \vec{F}^B + {}^N\underline{C}^B \cdot \vec{G}_h^{\,B}\delta(\tau - t_{k_h}) = m_B\ddot{\vec{x}}_B \tag{8}$$

Poisson's Kinematical Equations

$$ {}^{N}\dot{\underline{C}}^{B} = {}^{N}\underline{C}^{B} \cdot [{}^{N}\underline{\omega}^{B}\times]_{B} \tag{9} $$

where ${}^{N}\vec{\Omega}^{B} = {}^{N}\vec{\omega}^{B} + \dot{\vec{\phi}}$ with ${}^{N}\vec{\omega}^{B}$ being the angular velocity of the the despun reference frame with respect to the Newtonian frame N and $\dot{\vec{\phi}}$ being the spin rate of the lightcraft body about its axis of symmetry relative to the despun reference frame.[4] It is assumed that there are several impulsive loads H_{i_h}, G_{i_h} applying on the body at times t_{k_h}. Note indicial notation is being used (i.e. summation over repeated indices is implied). Utilizing the procedure outlined above, the follow relations associated with the i-th local (i=1,2,3 body fixed) directions are achieved.

Impulsive state-time representation of Euler's equations

$$ \begin{array}{l} H_{1_h}\psi_r(t_{k_h}) - I_{11}\left\{\left[\bar{q}_{1_u}\dot{\psi}_u(t_f)\cdot\psi_r(t_f) - \omega_1(t_0)\cdot\psi_r(t_0)\right] - \right. \\ \left.\bar{q}_{1_u}\int_{t_0}^{t_f}\dot{\psi}_u(\xi)\cdot\dot{\psi}_r(\xi)d\xi\right\} \approx 0 \end{array} $$

$$ \begin{array}{l} H_{2_h}\psi_r(t_{k_h}) - I_{22}\left\{\left[\bar{q}_{2_v}\dot{\psi}_v(t_f)\cdot\psi_r(t_f) - \omega_2(t_0)\cdot\psi_r(t_0)\right] - \right. \\ \left.\bar{q}_{2_v}\int_{t_0}^{t_f}\dot{\psi}_v(\xi)\cdot\dot{\psi}_r(\xi)d\xi\right\} - \bar{q}_{1_u}\cdot\bar{q}_{3_w}\cdot\left\{(I_{11}-I_{33})\int_{t_0}^{t_f}\dot{\psi}_u(\xi)\cdot \right. \\ \left.\dot{\psi}_w(\xi)\cdot\psi_r(\xi)d\xi\right\} - I_{11}\cdot\dot{\phi}\cdot\bar{q}_{3_w}\int_{t_0}^{t_f}\dot{\psi}_w(\xi)\cdot\psi_r(\xi)d\xi \approx 0 \end{array} \tag{10} $$

$$ \begin{array}{l} H_{3_h}\psi_r(t_{k_h}) - I_{33}\left\{\left[\bar{q}_{3_w}\dot{\psi}_w(t_f)\cdot\psi_r(t_f) - \omega_3(t_0)\cdot\psi_r(t_0)\right] - \right. \\ \left.\bar{q}_{3_w}\int_{t_0}^{t_f}\dot{\psi}_w(\xi)\cdot\dot{\psi}_r(\xi)d\xi\right\} - \bar{q}_{1_u}\cdot\bar{q}_{2_v}\cdot\left\{(I_{22}-I_{11})\int_{t_0}^{t_f}\dot{\psi}_u(\xi)\cdot \right. \\ \left.\dot{\psi}_v(\xi)\cdot\psi_r(\xi)d\xi\right\} + I_{11}\cdot\dot{\phi}\cdot\bar{q}_{2_v}\int_{t_0}^{t_f}\dot{\psi}_v(\xi)\cdot\psi_r(\xi)d\xi \approx 0 \end{array} $$

Impulsive state-time representation of Newton's 2^{nd} law

$$ \begin{array}{l} m\left\{\left[\bar{x}_{1_j}\dot{\psi}_j(t_f)\cdot\psi_r(t_f) - \dot{x}_1(t_0)\cdot\psi_r(t_0)\right] - \bar{x}_{1_j}\int_{t_0}^{t_f}\dot{\psi}_j(\xi)\cdot\dot{\psi}_r(\xi)d\xi\right\} - \\ \psi_{rx}(t_{k_h})\left[\bar{C}_{11_x}G_{1_h} + \bar{C}_{12_x}G_{2_h} + \bar{C}_{13_x}G_{3_h}\right] + \bar{C}_{11_x}mg\int_0^1\psi_r(\xi)d\xi \approx 0 \end{array} $$

$$ \begin{array}{l} m\left\{\left[\bar{x}_{2_j}\dot{\psi}_j(t_f)\cdot\psi_r(t_f) - \dot{x}_2(t_0)\cdot\psi_r(t_0)\right] - \bar{x}_{2_j}\int_{t_0}^{t_f}\dot{\psi}_j(\xi)\cdot\dot{\psi}_r(\xi)d\xi\right\} - \\ \psi_{rx}(t_{k_h})\left[\bar{C}_{21_x}G_{1_h} + \bar{C}_{22_x}G_{2_h} + \bar{C}_{23_x}G_{3_h}\right] \approx 0 \end{array} \tag{11} $$

$$ \begin{array}{l} m\left\{\left[\bar{x}_{3_j}\dot{\psi}_j(t_f)\cdot\psi_r(t_f) - \dot{x}_3(t_0)\cdot\psi_r(t_0)\right] - \bar{x}_{3_j}\int_{t_0}^{t_f}\dot{\psi}_j(\xi)\cdot\dot{\psi}_r(\xi)d\xi\right\} - \\ \psi_{rx}(t_{k_h})\left[\bar{C}_{31_x}G_{1_h} + \bar{C}_{32_x}G_{2_h} + \bar{C}_{33_x}G_{3_h}\right] \approx 0 \end{array} $$

State-time representation of Poisson's kinematical equations

$$ \begin{array}{l} \bar{C}_{il_n}\cdot\int_{t_0}^{t_f}\dot{\psi}_n(\xi)\psi_r(\xi)d\xi + \\ \bar{C}_{im_j}\cdot\left\{\varepsilon_{mlk}\bar{q}_{k_p}\int_{t_0}^{t_f}\dot{\psi}_p(\xi)\cdot\psi_j(\xi)\cdot\psi_r(\xi)d\xi\right\} \quad \approx \quad 0 \end{array} \tag{12} $$

Equations (10), (11), and (12) represent the state-time representation of the lightcraft equations of motion, which constitute $15\cdot k\cdot n_e$ nonlinear algebraic equations and unknowns. k represents the order of the polynomial interpolation functions utilized and n_e denotes the number of temporal elements. The barred quantities are the state-time variables to be solved for. The state of the system can be determined by substituting the state-time variables into the following interpolating relations.

$$ \begin{array}{lll} x_i \rightarrow \bar{x}_{i_\alpha}\psi_\alpha(t) & ; & \dot{x}_i \rightarrow x_{i_\alpha}\dot{\psi}_\alpha(t) \\ C_{ij} \rightarrow \bar{C}_{ij_\gamma}\psi_\gamma(t) & ; & \dot{q}_i \rightarrow q_{i_\beta}\dot{\psi}_\beta(t) \end{array} \tag{13} $$

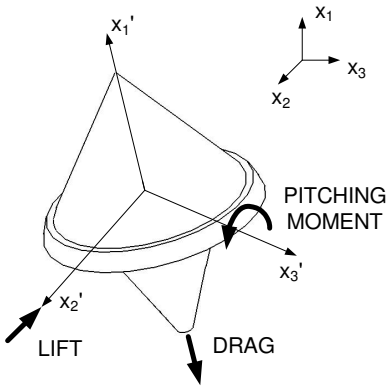

Figure 3. Aerodynamic Forces on the Lightcraft

V. Treatment of Aerodynamic Forces

Aerodynamic forces are important factors in the dynamic behavior of the lightcraft. Thus, it is necessary to develop an appropriate aerodynamic model in order to adequately represent the behavior of the vehicle. The three most important aerodynamic forces affecting the lightcraft are lift, drag, and pitching moment. As the lightcraft is not a traditional air vehicle, these forces act in an unconventional sense. Consequently, aerodynamic considerations of the lightcraft are more similar to a rocket in this fashion.[5] The drag tends to slow the vehicle down, the lift is a side force which is used to stabilize and control the direction of flight, and the pitching moment tends to tip the vehicle, as illustrated in Fig. 3.

The aerodynamic lift and drag as well as the pitching moment acting on the lightcraft are given respectively as below

$$\begin{aligned} L &= \tfrac{1}{2}\rho v^2 S c_L \\ D &= \tfrac{1}{2}\rho v^2 S c_D \\ M &= \tfrac{1}{2}\rho v^2 S c_M \end{aligned} \tag{14}$$

In these expressions, v is the lightcraft speed, ρ is the air density, and S is the lightcraft planform area. The air density and lightcraft planform area are both assumed constant. The coefficients of lift c_L, drag c_D, and moment c_M are functions of angle of attack α. Through the use of a computational fluid dynamics software Fluent,[6] data has been produced relating these aerodynamic coefficients to α. By using the relation between the C_{11} element of the direction cosine matrix ${}^N C^B$ and the angle of attack α, $C_{11} = \cos(\alpha)$, a quadratic regression fit can be utilized to produce the following expressions

$$\begin{aligned} c_L &= l_0 + l_1 C_{11} + l_2 C_{11}^2 \\ c_D &= d_0 + d_1 C_{11} + d_2 C_{11}^2 \\ c_M &= m_0 + m_1 C_{11} + m_2 C_{11}^2 \end{aligned} \tag{15}$$

Substituting Eqn. (15) in Eqn. (14) causes these equations to become quartic in system state variables, which is not desirable within the state-time methodology as the approach attempts to produce a set of algebraic equations with a minimum degree of nonlinearity. As evidenced in experiment and in previous data presented on the lightcraft,[3] the state variables do not undergo large variations in magnitude between impulses. Thus, it is legitimate to linearize these high-order aerodynamic terms about the previous impulse between successive impulses. This simplification is accomplished in a manner similar to that of sliding linearization schemes in control algorithms.[7]

As lift is a function of speed and the angle of attack, where each of these two quantities are dependent on time, one can write the following expression for lift.

$$L(t) = L(v(t), C_{11}(t)) \tag{16}$$

Consider the following first-order Taylor series expansion for $L(t + \Delta t)$.

$$\begin{aligned} L(t+\Delta t) &= L(v(t)+\Delta v, C_{11}(t)+\Delta C_{11}) \\ &\approx L(v(t), C_{11}(t)) + \frac{dL}{dv}(t)\Delta v + \frac{dL}{dC_{11}}(t)\Delta C_{11} \end{aligned} \tag{17}$$

In the above equation,

$$\begin{aligned} \tfrac{dL}{dv}(t) &= \rho v(t) S(l_0 + l_1 C_{11}(t) + l_2 (C_{11}(t))^2) \\ \tfrac{dL}{dC_{11}}(t) &= \tfrac{1}{2}\rho v(t)^2 S(l_1 + 2 l_2 C_{11}(t)) \end{aligned} \tag{18}$$

In order to solve the state-time equations of motion, one must use a nonlinear algebraic equation solver such as the Newton-Raphson scheme. Such solvers require an initial guess for the variables to start the iteration. The presence of these initial estimates for the state variables, as well as the small variations of these variables between impulses, allows us to treat $L(v(t), C_{11}(t))$, $\frac{dL}{dv}(t)$, and $\frac{dL}{dC_{11}}(t)$ as known constants in Eqn. (17) thus reducing it to a linear form for the entire time domain before the next impulse occurs.

With the above considerations, a linearization scheme can be developed for the aerodynamic forces. Let t_{k_h} denote a time at which an impulse occurs. As the state variables experience a large variation in magnitude at this instant, there happens a large increase in the lift as well. Hence, at this particular time Eq. (14) must be used to express the lift. However, for all subsequent temporal nodes, the linearized form of the lift, Eq. (17), about time $t = t_{k_h}$ should be utilized. Consequently, lift becomes quartic in system state variables at the impulse nodes and linear elsewhere. A similar discussion can be made for the drag and pitching moment.

We now discuss the inclusion of aerodynamic forces into the state-time equations of motion. First, let us consider Eqns. (19) and (20) with aerodynamic terms.

Euler's equations with aerodynamic terms

$$M\hat{e_3} + \vec{H_h}^{B/B^*}\delta(\tau - t_{k_h}) = \vec{\bar{I}}^{B/B^*} \cdot^N \vec{\alpha}^B + {}^N\underline{\Omega}^B \times \vec{\bar{I}}^{B/B^*} \cdot^N \vec{\omega}^B \tag{19}$$

Newton's 2^{nd} law with aerodynamic terms

$${}^N\underline{C}^B \cdot (-L\hat{e_2} - D\hat{e_1} + \vec{F}^B) + {}^N\underline{C}^B \cdot \vec{G_h}^B \delta(\tau - t_{k_h}) = m_B \ddot{\vec{x}}_B \tag{20}$$

where $\hat{e^1}$ and $\hat{e^2}$ are unit vectors in the directions opposite of the drag and lift forces respectively.

Since the new equations are highly similar in form to one another, only one of the above state-time equations of motion, namely the x_1-component of Newton's 2^{nd} law, is shown below. The others may be treated similarly. Before the application of a linearization scheme, the state-time form of the x_1-component of Newton's 2^{nd} law is

$$\begin{aligned} &m\left\{\left[\bar{x}_{1_j}\dot{\psi}_j(t_f)\cdot\psi_r(t_f) - \dot{x}_1(t_0)\cdot\psi_r(t_0)\right] - \bar{x}_{1_j}\int_{t_0}^{t_f}\dot{\psi}_j(\xi)\cdot\dot{\psi}_r(\xi)d\xi\right\} - \\ &\psi_{rx}(t_{k_h})\left[\bar{C}_{11_x}G_1 + \bar{C}_{12_x}G_2 + \bar{C}_{13_x}G_3\right] + \bar{C}_{11_x}mg\int_{t_0}^{t_f}\psi_r(\xi)d\xi - \\ &\tfrac{1}{2}\rho S\int_{t_0}^{t_f}((\bar{x}_{1_j}\dot{\psi}_j(\xi))^2 + (\bar{x}_{2_k}\dot{\psi}_k(\xi))^2 + (\bar{x}_{3_l}\dot{\psi}_l(\xi))^2)\cdot[l_0 + \\ &l_1\bar{C}_{11_m}\psi_m(\xi) + l_2(\bar{C}_{11_m}\psi_m(\xi))^2]\cdot\bar{C}_{12_n}\psi_n(\xi)\cdot\psi_r(\xi)d\xi - \\ &\tfrac{1}{2}\rho S\int_{t_0}^{t_f}((\bar{x}_{1_j}\dot{\psi}_j(\xi))^2 + (\bar{x}_{2_k}\dot{\psi}_k(\xi))^2 + (\bar{x}_{3_l}\dot{\psi}_l(\xi))^2)\cdot[d_0 + \\ &d_1\bar{C}_{11_m}\psi_m(\xi) + d_2(\bar{C}_{11_m}\psi_m(\xi))^2]\cdot\bar{C}_{11_n}\psi_n(\xi)\cdot\psi_r(\xi)d\xi \approx 0 \end{aligned} \tag{21}$$

Thus, the lift and drag contributions are pentic expressions in the state-time variables. As described above, Eq. (21) only needs to be applied at the nodes where an impulse occurs. At the nodes located between impulses, one linearizes the lift and drag about the previous impulse node which results in a set of equations with reduced order in nonlinearity. As the linearized equations become quite lengthy due to linearization about four variables (specifically, the displacement and Direction Cosine variables) and are not felt to add significantly to the presentation of the method in this application, the authors have elected to omit placing these equations in the text of the paper. It is worth noting, however, that the resulting set of equations are quadratic expressions in the state-time variables, and as such, are much more well-behaved in a nonlinear algebraic equation solver.

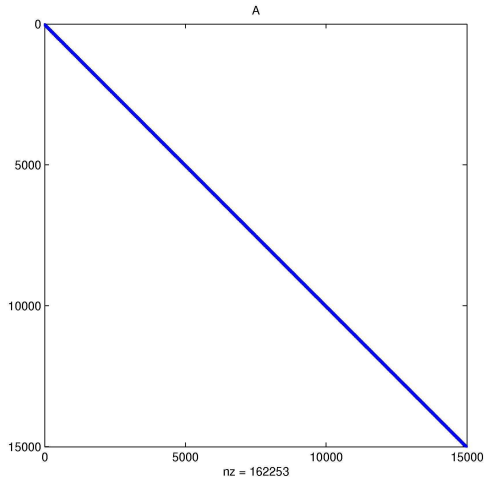

Figure 4. The Sparse, Near-Diagonal Structure of the System Tangent Matrix

VI. Simulation and Results

A Newton-Raphson type iterative scheme can be used to solve for the state-time variables appearing in Eqn.'s (10-12) with associative aerodynamic terms as discussed above. The tangent (Jacobian) matrix associated with these equations which is realized by linearizing these equations about the current iterate is very sparse, near-diagonal, and unsymmetric. This is demonstrated in Fig. 4. Such a sparse structure lends itself especially well to skyline matrix storage and parallel sparse iterative solvers such as those included in the PETSc software package.[8] However, the results presented in this paper are obtained by running the simulation in Matlab.

An initial guess is necessary for the Newton-Raphson iterative scheme. As the aerodynamic terms add quintic nonlinearities at the impulse nodes, it is important that a satisfactory initial guess is chosen. A variety of methods may be employed to accomplish this such as Genetic Algorithms. Genetic Algorithms, while quite parallelizable, are slow to reach an accurate initial guess. A favorable alternative, then, is to use continuation.[9] In the proposed continuation procedure, Eqn.'s (10-12) are first solved without the inclusion of aerodynamic forces. Then, the aerodynamic contributions are gradually introduced. Specifically, one introduces a continuation vector, denoted

$$c = \{c_0, c_1, \cdots, c_n\} \tag{22}$$

such that $c_0 < c_1 < \cdots < c_n$, $c_0 = 0$, and $c_n = 1$. Then, one defines intermediate numerical aerodynamic coefficients as

$$\begin{aligned} d_{i_j} &= c_j d_i \\ l_{i_j} &= c_j l_i \\ m_{i_j} &= m_j l_i \end{aligned} \tag{23}$$

for $i = 1, 2, 3$ and $j = 0, 1, \cdots, n$. A numerical scheme is divided into $n + 1$ stages. At the $j + 1^{th}$ stage, one solves Eqn.'s (10-12) along with aerodynamic forces with coefficients defined by d_{i_j}, l_{i_j}, and m_{i_j} for $i = 1, 2, 3$. As an initial condition, the result from solving the equations at the j^{th} stage is utilized provided $j \neq 0$. By using this continuation procedure, one only needs to determine an initial condition for the case $j = 0$. At this stage, however, the resulting system of equations is at worst quadratic and a much less accurate guess is required. For the lightcraft model, the stability of the continuation-based Newton-Raphson iterations was tested for fairly random initial guesses. Using $n = 2$ and an evenly distributed continuation vector, the iterations converged in merely 2-3 iterations per continuation stage for most initial conditions and impulses. In fact, convergence was never slower than 5 iterations for an individual continuation stage. This result shows much promise for future implications of the state-time methodology.

A flow chart for the resulting simulation scheme is presented in Fig. 5. There are a few specific details not mentioned in this figure which will now be discussed. These issues are: (i) generation of initial guess, (ii) tangent matrix formation, and (iii) linear system solution.

A. Generation of Initial Guess

As discussed above, there are many methods for the generation of an appropriate initial guess. Evolutionary algorithms are particularly useful. Genetic algorithms are one technique investigated in recent years for the solution of dynamic systems.[10] While this technique is useful for obtaining an initial guess in the local neighborhood of the solution, it has a very slow convergence rate. In this paper, all of the simulations use an initial guess which is the solution to the unforced lightcraft problem. In the unforced problem, gravity and aerodynamics are ignored. An analytical solution is easily derived. While this initial guess is not incredibly accurate, through extensive numerical testing, it was found that this estimate was sufficient.

B. Tangent Matrix Formation

The formation of the tangent matrix in the code employed is similar to that of conventional finite element algorithms.[11] This approach is computationally efficient and fast. Each temporal element is mapped to a corresponding parent element. The formation of the residual and tangent matrix is then first done in the parent element and then mapped back to the temporal element. Integration is accomplished through the use of Gaussian quadrature. A loop is done over the temporal elements, and for each of these elements, an element tangent matrix and residual is created. Finally, an assembly operation is executed, assimilating the element tangent matrices and residual vectors into the global tangent matrix and residual vector.

C. Linear System Solution

The equations above result in a system of nonlinear algebraic equations. In the Newton iterative scheme, a linearization of this equations is executed, and the resulting system of linear equations is

$$\mathbf{K}u = r \tag{24}$$

where $\mathbf{K}$ is the system tangent matrix, r is the residual vector, and u is a correction vector to solve. In the previous section, the formation of $\mathbf{K}$ and r was discussed. A streamlined approach was utilized in order to minimize the cost associated with this formation. Solving this system can also be prohibitively expensive. However, there are a number of computationally fast approaches for solving this sparse system. In the Matlab code, a GMRES[12] (Generalized Minimum Residual) method is utilized. GMRES is a sparse iterative solver for the solution of unsymmetric problems. Generally, a few hundred iterates of GMRES resulted in an accurate solution to the above equation.

D. Results and Discussion

A 3 second simulation of the laser-powered lightcraft was completed using both the discussed linearized state-time formulation and a traditional formulation using Autolev software[13] where the same initial full dynamics (containing full nonlinear dynamics and aerodynamics terms) strong form was considered. In this simulation, realistic values were chosen for the aerodynamic parameters, lightcraft spin rate, and initial conditions based on a particular experimental study conducted in New Mexico by the United States Air Force.[3] Furthermore, quadratic Lagrangian shape functions were utilized to interpolate the state-time variables. A comparison of the results from the state-time and traditional time-marching algorithms with the experimental results is provided in Fig. 6. In this figure, one notices that the linearized state-time algorithm provides consistent results with the tradtional time-marching and experimental results. The linearized state-time algorithm does, however, predict slightly higher flights than those predicted using the same initial model (governing differential equations) solved using a traditional time-marching procedure. This is because the sliding linearization used in estimating the aerodynamic lift, drag, and moment slightly under approximates these terms. This is as expected as the linearized form is linearly dependent on velocity rather than quadratically dependent.

In Fig. 7, the simulated vertical speed, and drag time histories are presented. From these two plots, one observes sawtooth behavior in the solution curve. This is as expected. At each impulse, there is a jump in the velocity and a corresponding jump in the drag. Then, as drag and gravity affect the lightcraft,

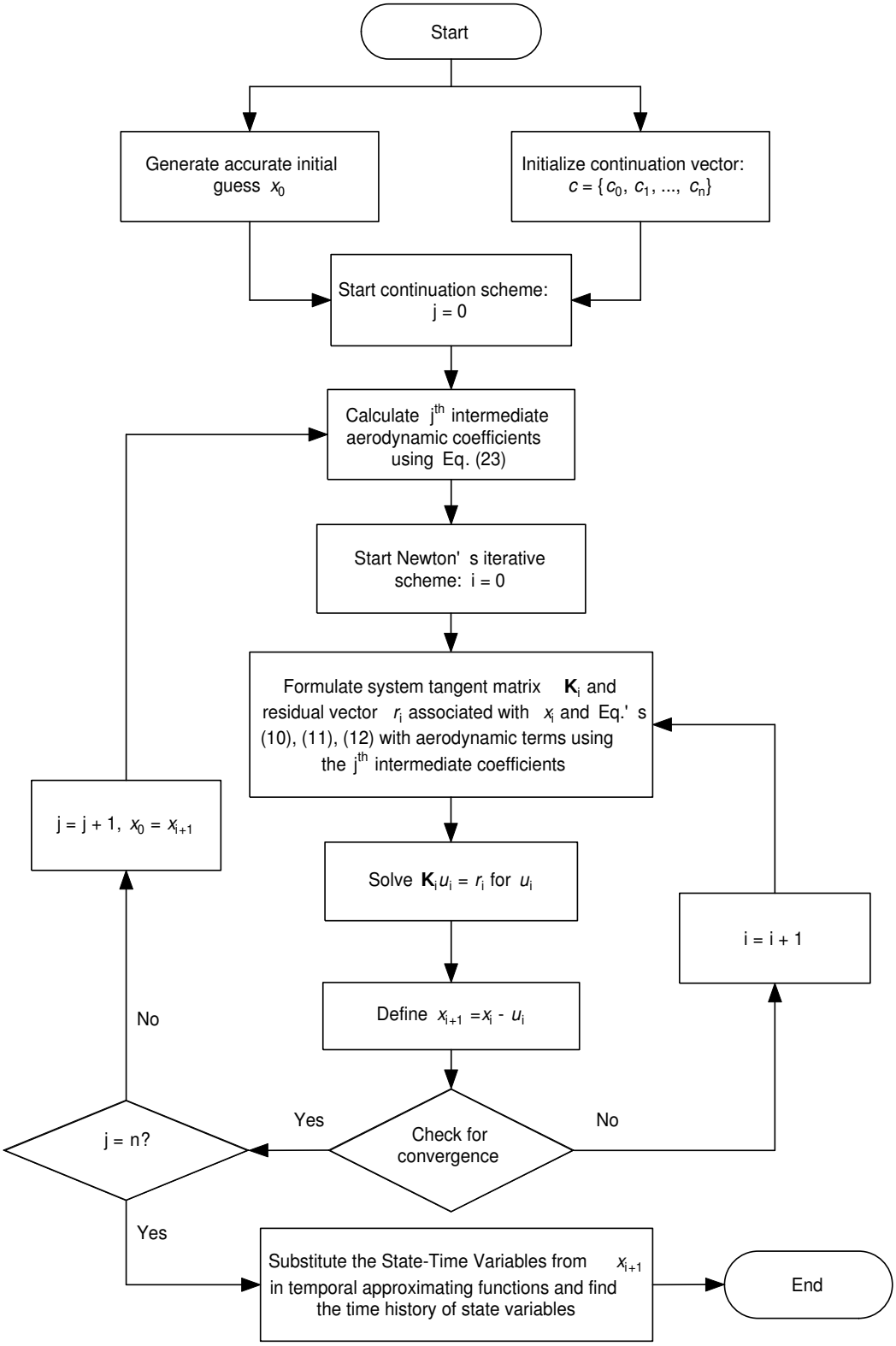

Figure 5. Flow chart of linearized state-time simulation utilizing continuation

the velocity drops and so does the corresponding drag. Finally, in Fig. 8, results for the angular velocity from a slightly different simulation are presented. In this simulation, the initial spin rate of the lightcraft is

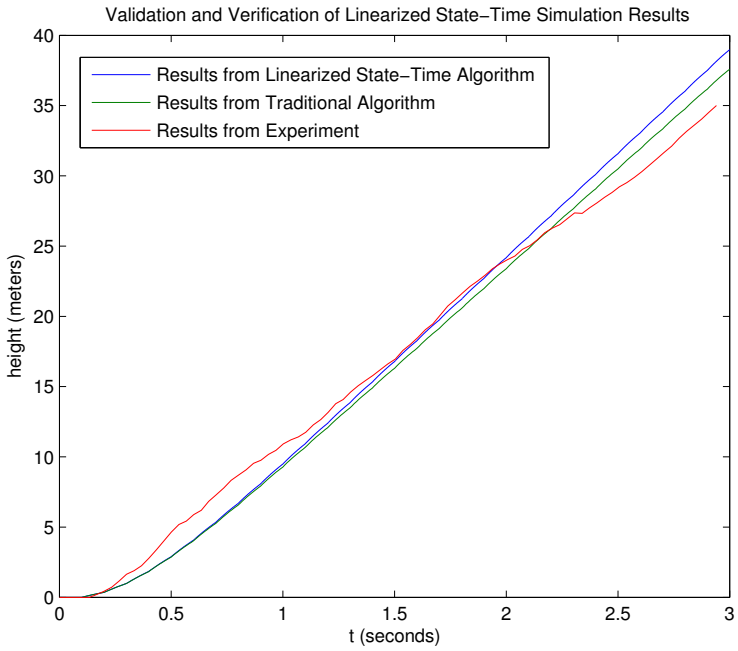

Figure 6. Comparison of lightcraft height after 3 seconds as determined by linearized State-Time algorithm, traditional time-marching scheme, and experiment

decreased by a factor of about 10 in order to visually reveal the impulse effects on angular velocity. In the plot, one observes proper capturing of the spin rate and jumps in the angular velocity at each impulse node as expected.

Note that in these diagrams the presented state-time formulation correctly captures the velocity jumps both in translation and rotation which result from the laser impulses. This is made achievable by two facts. First, the state-time equations are written on the position/orientation level. This enforces continuity on position but allows discontinuities at the velocity and acceleration levels at the element boundaries. Second, as the impulses occur at times known a priori, the locations of temporal elements can be placed such that the impulses occur at a boundary between temporal elements. For future consideration, one could conceivably eliminate the need for a priori domain discretization via utilizing either wavelet basis functions or a discontinuous Galerkin method.

One also notes the large number of temporal elements used in this problem; this particular problem requires a large number of temporal elements in order to capture the rapid coning behavior of the lightcraft. In order to capture only 0.5 seconds of simulation time at a reduced spin rate of 100 Radians per second, nearly 500 temporal elements should be used. If quadratic Lagrange shape functions are adopted to interpolate the system state variables, the resulting system consists of 15,000 equations and unknowns. In order to capture the behavior of the lightcraft and its true spin rate for 15 seconds, one needs to use about 135,000 to 140,000 temporal elements, or more than 4,000,000 equations and unknowns. A comparable number of integration time steps N_{steps} would be required using a conventional time-marching scheme integrating the system equations of motion. As this problem involves only six degrees of freedom, the simulation turnaround that one can achieve through parallel time-marching state dynamics algorithms is theoretically $T_{simulation} = N_{steps} \cdot O(\log_2 n) = 10^5\, O(\log_2 6) \sim O(10^5)$. On the other hand, if one assumes that there are sufficiently many processors (with ideal communication) available, the state-time approach would offer the possibility of reducing simulation turnaround time to $T_{simulation} = O(\log_2 N_{elements}) + O(\log_2 n) = O(\log_2 10^5) + O(\log_2 6) \sim O(20)$.

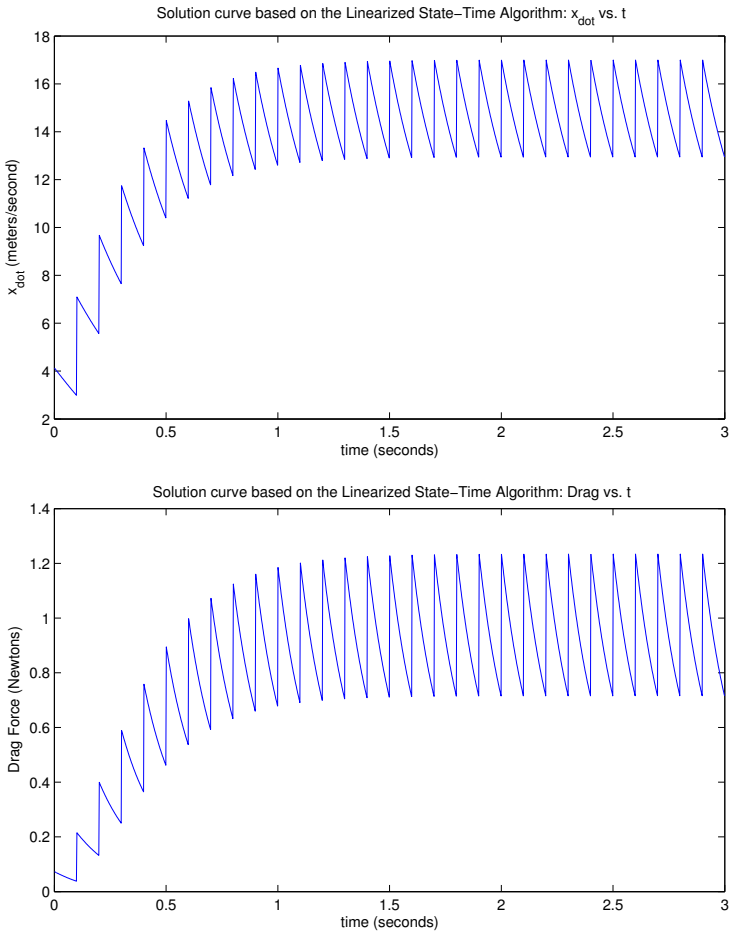

Figure 7. Velocity and drag state-time results over 3 seconds

VII. Future Work

Parallelization of the state-time lightcraft code is currently under development by the authors at the Computational Dynamics Laboratory at Rensselaer Polytechnic Institute. There are three main areas where parallelization is possible. The first of these is in the generation of an accurate initial guess. Genetic Algorithms are an efficient approach to generating initial estimates for the solution of a dynamic system, and as these algorithms consist of mutating an independent population, they are inherently parallel. Next, parallelization is a key aspect in tangent matrix and residual vector formation. In fact, every operation in the formation can be done simultaneously. Traditionally, the formation of element mass matrices and residual vectors is distributed among processors, and assembly is conducted on a master processor. Finally, parallelization is possible in the solution of the resulting linear system. Linear algebra libraries are readily available (PETSc, SuperLU) containing efficient parallel iterative sparse solvers. It is the hope of the authors that parallel implementation of the current algorithm would result in favorable speedup characteristics.

VIII. Conclusion

The state-time formulation is one of the first of its kind in the context of multibody system dynamics. Its ability to capture the entire temporal domain in one set of equations, and thus greatly extend the degree to which coarse grain parallelization may be realized, is ground-breaking. Nevertheless, verification and validation of the proposed methodology against traditional schemes and experimental data is necessary.

In this paper, a state-time model for the Type 200 lightcraft is presented. To model the vehicle using this methodology in an optimal manner, a modified formulation is derived to account for impulse forces.

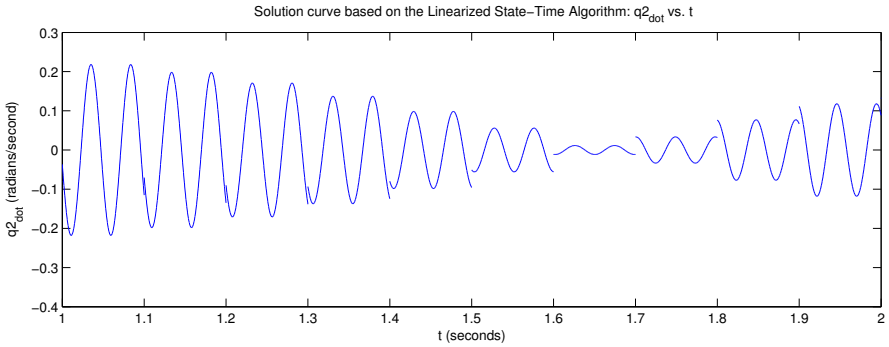

Figure 8. Angular velocity state-time results for a reduced spin rate

This formulation allows parallelization over the entire temporal domain, including across impulses. An aerodynamic model compatible with the proposed formulation is also introduced in which to reduce the dimensionality of the equations, and a sliding linearization scheme similar to those used in control applications is used to reduce aerodynamic terms from quartic to locally linear. Finally, state-time simulation results are presented and compared to results obtained from Autolev software and experimental data.

Acknowledgments

Special thanks to Professor Leik Myrabo of Rensselaer who is overseeing the lightcraft effort and who has supplied us with all our lightcraft mass properties and aerodynamic data. Thank you also to Mr. Chris Ballard of the Rensselaer Computational Dynamics Laboratory who has provided all of the lightcraft simulation results obtained via traditional time-marching methods. Finally, support for this work has been provided by National Science Foundation (NSF) under the Award No. CMS-0219734 and is gratefully appreciated.

References

[1]Anderson, K. S. and Oghbaei, M., "Dynamic Simulation of Multicomponent Systems Using a New State-Time Methodology," *Multibody System Dynamics*, Vol. 14, 2005, pp. 61–80.

[2]Anderson, K. S. and Oghbaei, M., "A State-Time Formulation for Dynamic Systems Simulation Using Massively Parallel Computing Resources," *Nonlinear Dynamics*, Vol. 39, No. 3, 2005, pp. 305–318.

[3]Myrabo, L., "World Record Flights of Beam-Riding Rocket Lightcraft: Demonstration of 'Disruptive' Propulsion Technology," *37th AIAA/ASME/SAE/ASEE Joint Propulsion Conference*, Salt Lake City, Utah, July 2001, AIAA Paper N. 2001-3798.

[4]Meriam, J. L., *Dynamics: Second Edition, SI Version*, John Wiley and Sons Inc., New York, NY, 1975.

[5]Ketchledge, D. A., "Actice guidance and dynamic flight mechanics for model rockets," *High Power Rocketry*, July-Aug. 1993, pp. 1–30.

[6]URL http://www.fluent.com/.

[7]L. R. Hunt, R. S. and Meyer, G., "Global transformation of nonlinear systems," *IEEE Transaction on Automatic Control*, , No. 1, Jan. 1983, pp. 24–31.

[8]URL http://acts.nersc.gov/tools.html.

[9]Ascher, U. M. and Petzold, L. R., *Computer Methods for Ordinary Differential Equations and Differential-Algebraic Equations*, Society of Industrial and Applied Mathematics, Philadelphia, 1998.

[10]Diver, D. A., "Applications of genetic algorithms to the solution of ordinary differential equations," *Journal of Physics A: Mathematical and General*, July 1993, pp. 3503–3513.

[11]Hughes, T. J. R., *The Finite Element Method–Linear Static and Dynamic Finite Element Analysis*, Dover Publications, New York, 2000.

[12]Trefethen, L. N. and D. Bau, I., *Numerical Linear Algebra*, Society of Industrial and Applied Mathematics, Philadelphia, 1997.

[13]C.G. Ballard, K. A. and Myrabo, L., "Flight Dynamics Simulation of Lightcraft Propelled by Laser Ablation," *To be submitted to the AIAA Journal of Guidance, Control, and Dynamics*, 2006.